Analytical solutions for steady groundwater flow through aquifer folds and faults

Bakker, Mark; Anderson, Erik

DOI
10.1007/s10665-024-10405-8

Publication date
2024

Document Version
Final published version

Published in
Journal of Engineering Mathematics

Journal of Engineering Mathematics (2024) 149:4
https://doi.org/10.1007/s10665-024-10405-8

Analytical solutions for steady groundwater flow through aquifer folds and faults

Mark Bakker[1] · **Erik Anderson**[2]

Received: 10 June 2024 / Accepted: 30 September 2024 / Published online: 30 October 2024

Abstract
Deformations of the earth's crust create tortuous paths for groundwater flow, altering pressure distributions and flow lines. A solution for steady groundwater flow through a deformed aquifer is derived by applying the singular point method using a rectangular reference plane. The singular point method is used to develop conformal mappings with complex geometries using basic principles of groundwater mechanics including superposition, the method of images, and stagnation point analysis. The derived solution contains three parameters that can be chosen to simulate flow through a variety of deformed aquifers, including flow through a normal fault with a 90° dip, flow through a fold, and flow through a relay ramp.

Keywords Analytical · Conformal mapping · Faults · Folds · Groundwater

1 Introduction

Movement of the earth's crust creates complex shear zones, faults, folds, and deformation bands. These features impact fluid flow both by changing flow paths and by altering the hydraulic properties of the crust [1–6]. Analytical investigations of groundwater flow through faults with altered hydraulic properties have been made by Haneberg [7] who considered one-dimensional flow through a fault zone with altered hydraulic conductivity. Anderson [8] considered two-dimensional Dupuit flow through a linear fault, and Anderson and Bakker [9] investigated flow through a faulted multi-aquifer system, based on the Dupuit approximation. Numerous numerical studies of flow

Mark Bakker and Erik Anderson have contributed equally to this work.

✉ Mark Bakker
mark.bakker@tudelft.nl

Erik Anderson
eanderson@intera.com

[1] Water Management Department, Civil Engineering and Geosciences, Delft University of Technology, Stevinweg 1, 2628 CN Delft, Netherlands

[2] INTERA, Molly Brown Lane, Green Bay, WI 54313, USA

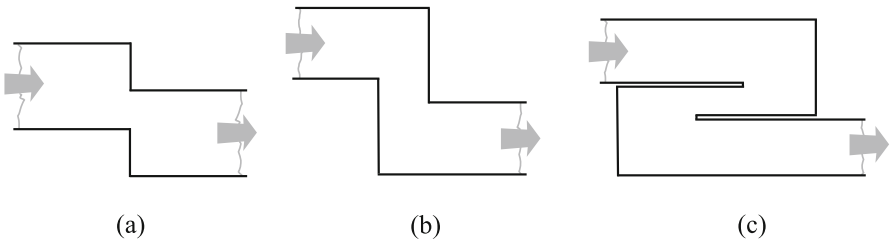

Fig. 1 Examples of flow through a deformed aquifer: **a** an aquifer offset by a fault in a vertical plane; **b** an isolated deformation band or shear zone in a vertical plane; **c** a fault relay ramp in a horizontal plane

through faulted or deformed aquifers exist, including Bense and Van Balen [10] who investigated regional flow through a faulted system, including the effects of fault relay ramps.

Even without changes to the hydraulic conductivity, the deformed geometry increases head losses and alters pressure and stress distributions. Cornelissen and Jansen [11] investigated the distribution of pore pressure in the vertical plane along a displaced normal fault, characterized by both a dip and offset; they used a numerical solution to the Schwarz–Christoffel transformation to solve the flow problem. Similarly, the impacts of the deformation of a simple homogeneous and confined aquifer on groundwater flow are considered here. The changing gradients and flow paths through the deformed region are examined without considering local changes in the hydraulic conductivity. Three idealized examples of deformed geometries are investigated, as presented in Fig. 1. The first example shows a fault similar to that studied by Cornelissen and Jansen [11], with a 90° dip.

A solution for steady groundwater flow through a deformed aquifer is derived by applying the singular point method of Chaplygin and Zhukovsky [12]. The method was originally developed to solve problems of free jets in ideal fluids by the hodograph method using a circular sector as a reference plane. The method is well suited to solve free boundary problems in groundwater flow [13–17]. The method is applied here to confined groundwater flow using a rectangular reference plane. The singular point method makes use of the basic principles of groundwater mechanics, including the method of images and the analysis of stagnation points, to develop the conformal mapping of the physical plane onto the plane of the complex potential.

Two-dimensional, potential flows for multiple wells in rectangular domains with various combinations of equipotential and impermeable boundaries have been long-investigated. Only a few examples within the field of groundwater mechanics are referenced here. Muskat [18] used the conduction sheet analog method to simulate direct-line, staggered-line, and five-spot line drive flood networks for oil recovery operations. Subsequently, the method of images with real analysis was used by Bear [19] and Mantoglou [20] to solve groundwater flow problems in a rectangular domain, by creating a doubly periodic lattice of image wells. Similar work using the method of images and complex analysis was performed more recently by Ding and Wang [21] who investigated multiple wells in a rectangular domain bounded by impermeable boundaries. Lu et al. [22] used complex analysis, the method of images and conformal

mapping to examine steady state pumping in rectangular aquifers with five different combinations of equipotential and impermeable boundaries. Wang et al. [23] solved the same suite of problems using real analysis and double Fourier transforms. Of the five combinations of boundary conditions considered by Lu et al. [22], four can be solved in parametric form using the Schwarz–Christoffel transformation. Many of those solutions can also be written directly without a parametric relationship [24]. Only the problem with parallel equipotentials and parallel impermeable boundaries cannot be solved by this approach, and the results must explicitly include an infinite sum of image wells.

The three main objectives of this paper are as follows:

1. Provide an alternate potential flow solution for wells in a rectangular domain bounded by parallel equipotentials and parallel impermeable boundaries.
2. Apply the singular point method to develop conformal mappings of the rectangular domain onto more complex domains, using basic concepts of groundwater mechanics.
3. Develop complete analytical solutions describing steady groundwater flow through deformed aquifers.

The paper starts with a problem statement and a description of the chosen rectangular reference pane. Next, general solutions are presented of the mapping of the reference plane onto the physical domain and the complex potential domain. Finally, the solution is applied to three specific groundwater flow problems: Flow through a vertical fault, flow through a fold, and flow through a fault relay ramp.

2 Problem statement

Consider the physical plane (z-plane) illustrated in Fig. 2, which presents a very general description of a deformed aquifer. This general geometry can be used to represent all three geometries illustrated in Fig. 1, as well as others, as special cases. Steady groundwater seepage occurs in the aquifer, entering on the left side of the deformed zone and exiting on the right side. All boundaries of the physical plane are impermeable and the total flow from left to right in the aquifer is constant and equal to U. The thickness of the aquifer is H_l on the left and H_r on the right of the deformed region. The base of the aquifer steps down by an amount a, while the top steps down by $H_l + a - H_r$ (see Fig. 2); the locations of the steps in aquifer base and top are offset by the horizontal distance b. The vertices of the physical plane are numbered 1 through 6 in Fig. 2, with vertices 1 and 4 lying at $x = \infty$ and $x = -\infty$, respectively; $z = x + \mathrm{i}y$ is the complex coordinate.

The two vertices P and S are branch points in the z-plane, and each lies at the end of a slot of infinitesimal width. As will be shown, the general solution allows these points to shift between the numbered vertices. For example, the figure shows vertex S lying at the end of a slot on boundary segment 5–6; alternately, S could lie on segment 4–5, rotating the slot by $-\pi/2$ and altering the shape of the physical plane. For clarity, the locations of points S and P will be treated as illustrated in Fig. 2 in the derivation

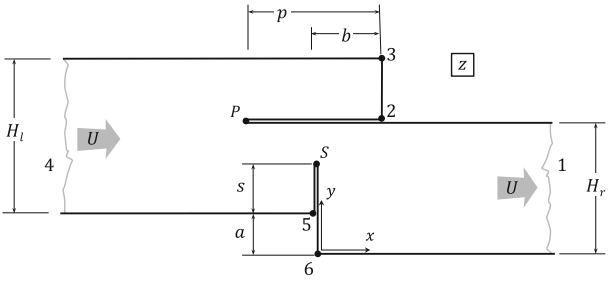

Fig. 2 The physical plane (z-plane)

of the solution; after the general solution is formulated, examples are provided that demonstrate alternate locations for these points.

Steady groundwater flow is governed by Laplace's equation. A solution is sought in the form of a complex potential $\Omega(z) = \phi + \mathrm{i}\psi$, where ϕ is the specific discharge potential and ψ is the stream function. The specific discharge potential is related to the hydraulic head h as $\phi = kh$, where k is the hydraulic conductivity. The x- and y-components of the specific discharge vector are obtained from the specific discharge potential as

$$q_x = -\frac{\partial \phi}{\partial x} \quad q_y = -\frac{\partial \phi}{\partial y}, \tag{1}$$

or in complex form as

$$W = q_x - \mathrm{i}q_y = -\frac{\mathrm{d}\Omega}{\mathrm{d}z}. \tag{2}$$

The solution $\Omega(z)$ must satisfy the following conditions along the boundaries of the physical plane:

$$1{-}2{-}3{-}4 : \Im\Omega = \psi_0, \tag{3}$$

$$4{-}5{-}6{-}1 : \Im\Omega = \psi_0 + U. \tag{4}$$

The notation 1–2–3–4 refers to the entire upper boundary of the aquifer from vertex 1 to 2 to 3 to 4. Similarly, 4–5–6–1 refers to the bottom boundary of the aquifer (vertex 4 to 5 to 6 to 1). Furthermore, $\Im$ indicates the imaginary part of a complex function, and ψ_0 is an arbitrary constant value. In addition, the real part of the complex potential is set to ϕ_0 at a reference point, z_0, to make the solution unique:

$$\Re\Omega(z_0) = \phi_0, \tag{5}$$

where z_0 is any location in the physical plane, where the head is known to be ϕ_0. The specific location chosen is not important—it only affects the value of equipotentials in the solution, but has no effect on the flow field.

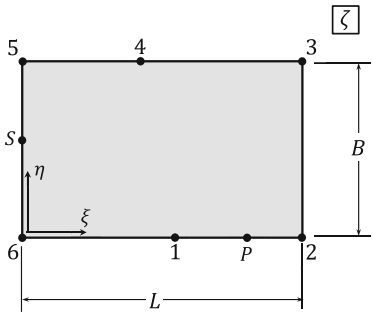

Fig. 3 The reference plane (ζ-plane)

An analytic solution to the stated problem is derived using conformal mapping. Introductions to conformal mapping in the context of groundwater flow can be found in, e.g., Verruijt [25], Strack [26], and Bakker and Post [27]. The derived solution will be in parametric form as $z(\zeta)$ and $\Omega(\zeta)$, where $\zeta = \xi + i\eta$ is the rectangular reference plane with length L and height B, illustrated in Fig. 3. The reference plane is chosen such that the two vertical sides of the rectangle correspond to the vertical sections 5–6 and 2–3, respectively, in the physical plane. Similarly, the piece-wise horizontal section 6–2 corresponds to the bottom of the rectangle and the piece-wise horizontal section 3–5 corresponds to the top of the rectangle. The exact locations of vertices 1, 4, P, and S are initially unknown in the reference plane, as well as the aspect ratio B/L of the rectangular reference plane, and must be evaluated to obtain a complete solution.

The parameters are evaluated from a non-linear system of conditions presented along with the solution. The system of conditions is then simplified by considering the three special cases introduced in Fig. 1, and flow nets are presented for each.

The mapping of the reference plane onto the physical plane, $z(\zeta)$

The mapping of ζ onto z has three degrees of freedom, which are chosen as follows: vertex 6 is placed at the origin ($\zeta_6 = 0$), vertex 2 is placed at a distance L along the real axis ($\zeta_2 = L$), and the shape of the ζ-plane is chosen to be a rectangle. The mapping is evaluated by identifying the singular behavior along the boundaries of the planes, building the behavior into the mapping, and applying the method of images for flow in a strip to satisfy all boundary conditions. As illustrated in Figs. 2 and 3, the conditions on z along the boundaries of the reference plane are as follows:

$$1{-}2 : \Im z = H_r, \tag{6}$$
$$2{-}3 : \Re z = b, \tag{7}$$
$$3{-}4 : \Im z = a + H_l, \tag{8}$$
$$4{-}5 : \Im z = a, \tag{9}$$
$$5{-}6 : \Re z = 0, \tag{10}$$
$$6{-}1 : \Im z = 0. \tag{11}$$

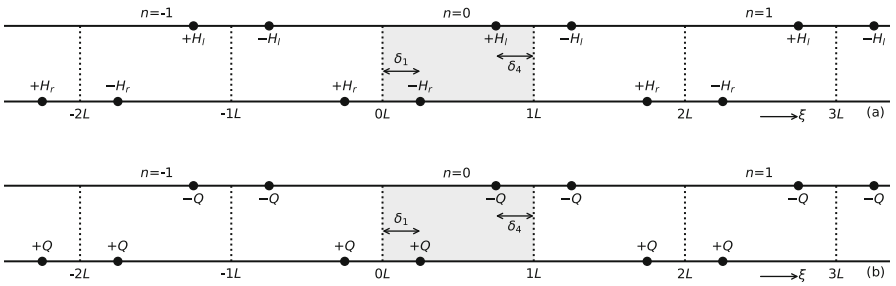

Fig. 4 Location and strength of images for $n = -1, 0, 1$. **a** Images for $z(\zeta)$ and **b** Images for $\Omega(\zeta)$

No singular behavior is observed at vertices 2, 3, 5, and 6. The mapping $z(\zeta)$ is conformal as the internal angle at the matching vertices equals $\pi/2$ in both the z-plane and the ζ-plane; no special behavior needs to be included in the mapping at these vertices. Vertices 1 and 4 both have a logarithmic behavior, as $\Im(z)$ jumps at both vertices; at vertex 1, the jump equals H_r, while at vertex 4, the jump equals minus H_l. Finally, conditions (7) and (10) show an offset of the real part of the two boundaries of value b.

The basic term in the mapping is the complex potential for a logarithmic singularity that creates a jump $-A$ at $\zeta = \zeta_d$ on the boundary of a horizontal, infinite strip of height B, which may be written as

$$\mathrm{F} = \frac{A}{\pi} \ln\left(\mathrm{e}^{\pi\zeta/B} - \mathrm{e}^{\pi\zeta_d/B}\right). \tag{12}$$

The vertex ζ_d may be located along the bottom ($\Im\zeta = 0$) or the top ($\Im\zeta = B$) of the strip. When ζ_d is on the bottom of the strip, the imaginary part of F equals A along the top of the strip and along the bottom of the strip to the left of ζ_d ($\Re\zeta < \Re\zeta_d, \Im\zeta = 0$), while it equals zero elsewhere along the boundary of the strip. Similarly, when ζ_d is on the top of the strip, the imaginary part of F equals A along the top of the strip to the right of ζ_d ($\Re\zeta > \Re\zeta_d, \Im\zeta = B$) and zero elsewhere along the boundary of the strip.

The mapping $z(\zeta)$ may be written, with the aid of function F, as

$$z(\zeta) = \frac{-H_r}{\pi} \ln\left(\mathrm{e}^{\pi\zeta/B} - \mathrm{e}^{\pi\zeta_1/B}\right) + \frac{H_l}{\pi} \ln\left(\mathrm{e}^{\pi\zeta/B} - \mathrm{e}^{\pi\zeta_4/B}\right) + f(\zeta), \tag{13}$$

where the first two terms to the right of the equal sign fulfill boundary conditions (6), (8), (9), and (11). In other words, these terms create the jumps in the imaginary part of the mapping at vertices 1 and 4, where ζ_1 and ζ_4 are the complex coordinates of vertices 1 and 4, respectively, in the ζ-plane. The function $f(\zeta)$ is analytic everywhere in the rectangle and on the boundary and will be chosen to fulfill boundary conditions (7) and (10), while not altering the other boundary conditions.

The function f, when combined with the other terms in (13), must satisfy conditions (6) through (11); the function is evaluated by direct application of the method of images about the two vertical boundaries of the reference plane. The method of images is applied by repeating the logarithmic singularities such that $\Re z$ is constant along the left

and right sides of the rectangular reference plane, as illustrated in Fig. 4a. Appropriate constants and linear functions are added such that $\Re z = 0$ along the left side of the reference plane and $\Re z = b$ along the right side.

$$z(\zeta) = \sum_{n=-\infty}^{\infty} \left\{ \frac{-H_r}{\pi} \ln\left[\frac{e^{\pi\zeta/B} - e^{\pi(2nL+\zeta_1)/B}}{e^{\pi\zeta/B} - e^{\pi(2nL-\zeta_1)/B}} \right] + \frac{H_r\delta_1}{B} \right\} - \frac{H_r\delta_1\zeta}{BL} + \sum_{n=-\infty}^{\infty} \left\{ \frac{H_l}{\pi} \ln\left[\frac{e^{\pi\zeta/B} - e^{\pi(2nL+\zeta_4)/B}}{e^{\pi\zeta/B} - e^{\pi(2nL-\zeta_4)/B}} \right] - \frac{H_l\delta_4}{B} \right\} + \frac{H_l\delta_4\zeta}{BL} + \frac{b}{L}\zeta + H_r\mathrm{i}, \tag{14}$$

where $\delta_1 = \Re\zeta_1$ and $\delta_4 = \Re\zeta_4$. Theoretically, an infinite number of images is required, but in practice a couple of images is sufficient to meet the boundary conditions up to machine accuracy.

Function (14) fulfills all boundary conditions (6) through (11). The values of H_l, H_r and b may be specified. The jump of the base a and the offsets p and s (i.e., the locations of points P and S) are determined by the choice of the height B of the rectangular reference plane and the locations of vertices ζ_1 and ζ_4 in the reference plane, as will be demonstrated in the following.

The functional form of the mapping has been constructed, but the physical dimensions of the z-plane must be related to the mapping parameters to complete the solution. The mapping of the reference plane onto the physical plane is not analytic in points P and S as the angle of the boundary at these corner points is not equal to the angle at the corresponding points in the reference plane. The points ζ_P and ζ_S are branch points in the z-plane and critical points in the ζ-plane; in potential flow these points are referred to as stagnation points. The function $z(\zeta)$ (14) is not analytic at these points, i.e., the derivative equals zero. The derivative of z is obtained from (14) as

$$z'(\zeta) = \frac{-H_r}{B} \sum_{n=-\infty}^{\infty} \left[\frac{1}{e^{\pi\zeta/B} - e^{\pi(2nL+\zeta_1)/B}} - \frac{1}{e^{\pi\zeta/B} - e^{\pi(2nL-\zeta_1)/B}} \right] - \frac{H_r\delta_1}{BL} + \frac{H_l}{B} \sum_{n=-\infty}^{\infty} \left[\frac{1}{e^{\pi\zeta/B} - e^{\pi(2nL+\zeta_4)/B}} - \frac{1}{e^{\pi\zeta/B} - e^{\pi(2nL-\zeta_4)/B}} \right] + \frac{H_l\delta_4}{BL} + \frac{b}{L}. \tag{15}$$

The location of points P and S in the reference plane may be obtained from the two conditions

$$z'(\zeta = \zeta_P) = 0, \tag{16}$$

$$z'(\zeta = \zeta_S) = 0. \tag{17}$$

Once the locations of points P and S are known, the values of the remaining parameters a, p, and s may be obtained from

$$z(\zeta = \zeta_P) = (b - p) + \mathrm{i}H_r, \tag{18}$$

$$z(\zeta = \zeta_S) = \mathrm{i}(a + s), \tag{19}$$

$$z(\zeta = \mathrm{i}B) = \mathrm{i}a, \tag{20}$$

where it is noted that $\zeta_5 = \mathrm{i}B$. Conditions (18) through (20) are a system of three non-linear algebraic equations that may be used to evaluate the parameters B, ζ_1, and ζ_4, completing the mapping $z(\zeta)$. In the second half of this paper, a number of practical cases are presented, where it is shown how to obtain a solution by choosing some of the parameters and by evaluating the others.

The mapping of the reference plane onto the plane of the complex potential, $\Omega(\zeta)$

The conditions on Ω along the boundary of the reference plane are given by (3) and (4); all boundaries are impermeable. The stream function is piece-wise constant along the boundary of the reference plane, with jumps of magnitude U occurring at vertices 1 and 4, indicating logarithmic behavior at these locations. This means that Ω may be written, with the aid of (12), as

$$\Omega(\zeta) = \frac{U}{\pi} \ln\left(\frac{\mathrm{e}^{\pi\zeta/B} - \mathrm{e}^{\pi\zeta_1/B}}{\mathrm{e}^{\pi\zeta/B} - \mathrm{e}^{\pi\zeta_4/B}}\right) + g(\zeta), \tag{21}$$

where function $g(\zeta)$ is analytic everywhere in the rectangle and on the boundary and will be chosen to fulfill boundary conditions along the left and right sides of the rectangular reference plane. The solution is again obtained with the method of images (see Fig. 4b)

$$\Omega(\zeta) = \frac{U}{\pi} \sum_{n=-\infty}^{\infty} \ln\left[\frac{(\mathrm{e}^{\pi\zeta/B} - \mathrm{e}^{\pi(2nL+\zeta_1)/B})(\mathrm{e}^{\pi\zeta/B} - \mathrm{e}^{\pi(2nL-\zeta_1)/B})}{(\mathrm{e}^{\pi\zeta/B} - \mathrm{e}^{\pi(2nL+\zeta_4)/B})(\mathrm{e}^{\pi\zeta/B} - \mathrm{e}^{\pi(2nL-\zeta_4/B)})}\right] + \Omega_0, \tag{22}$$

where Ω_0 is a complex constant to fulfill (3) and (5). Note that this problem, with wells and four impermeable boundaries, can be solved alternatively using Schwartz–Christoffel by mapping the rectangle onto the upper half-plane and applying the method of images in the upper half-plane, as discussed in the Sect. 1. To emphasize the approach used to evaluate $z(\zeta)$, the same approach is applied here to evaluate $\Omega(\zeta)$.

The presented solution is implemented in a Python script. A flow net illustrating the general solution $\Omega(z)$, using $z(\zeta)$ (14) and $\Omega(\zeta)$ (22), is provided in Fig. 5 for the case that $H_l = 0.5$, $H_r = 0.4$, and $b = 0.2$. The solution is evaluated in an inverse manner: The parameters in the ζ-plane are specified as $L = 1$, $B = 0.3$, $\zeta_1 = 0.05$, and $\zeta_4 = 0.6 + 0.3\mathrm{i}$. The parameters in the z-plane are evaluated from the results as $a = 0.14$, $p = 0.368$, and $s = 0.0743$.

3 Example 1: flow through a fault

The first example concerns flow through an aquifer with a vertical fault (Fig. 6). The thickness of the aquifer is equal to H on both sides of the fault ($H_r = H_l = H = 1$), the step in the base is a, and there is no offset ($b = 0$). Points 2 and P coincide ($p = 0$)

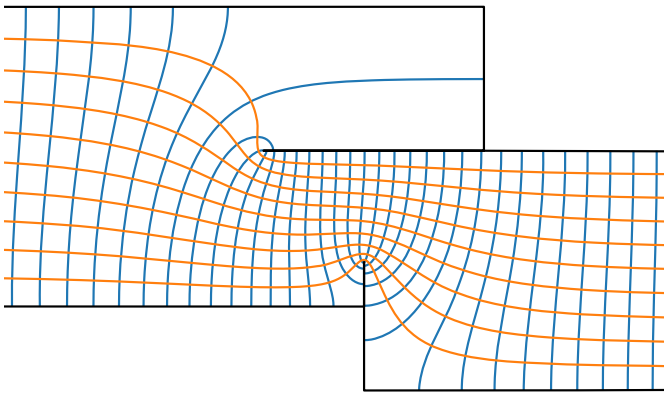

Fig. 5 Flow net for the case $H_l = 0.5$, $H_r = 0.4$, $b = 0.2$, $L = 1$, $B = 0.3$, $\zeta_1 = 0.05$, and $\zeta_4 = 0.6+0.3\mathrm{i}$. Blue lines are equipotentials and orange lines are streamlines

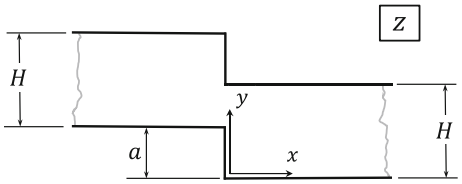

Fig. 6 Definition sketch of an aquifer in the vertical plane, offset by a normal fault of 90° dip

and points 5 and S coincide ($s = 0$). Point 1 is located along the bottom boundary of the rectangular reference plane at $\zeta_1 = \delta$. Because of symmetry, point 4 is located at $\zeta_4 = L - \delta + \mathrm{i}B$ along the top boundary of the reference plane. The conditions for evaluating the mapping parameters, (16) through (20), become

$$z'(\zeta = \zeta_2 = L) = 0, \tag{23}$$
$$z'(\zeta = \zeta_5 = \mathrm{i}B) = 0, \tag{24}$$
$$z(\zeta = L) = \mathrm{i}H, \tag{25}$$
$$z(\zeta = \mathrm{i}B) = \mathrm{i}a, \tag{26}$$
$$z(\zeta = \mathrm{i}B) = \mathrm{i}a. \tag{27}$$

Conditions (26) and (27) reduce to the same expression.

The length L of the rectangular reference plane and the location of point 1 are set to $L = 1$ and $\delta = 0.25$, respectively. The choice of δ determines the vertical jump a of the base at the fault (a smaller value of δ results in a larger jump a). Finally, the height of the rectangle B is adjusted such that the condition at point 5 (24) is met and by symmetry the condition at point 2 (23) using a standard root-finding algorithm, which gives $B = 0.63963$. Once the value of B is determined, the step in the base is computed from condition (26) as $a = 0.5$.

To better understand the solution, contours of x and y are drawn in the reference plane for three values of B in Fig. 7. The corresponding boundary of the domain and

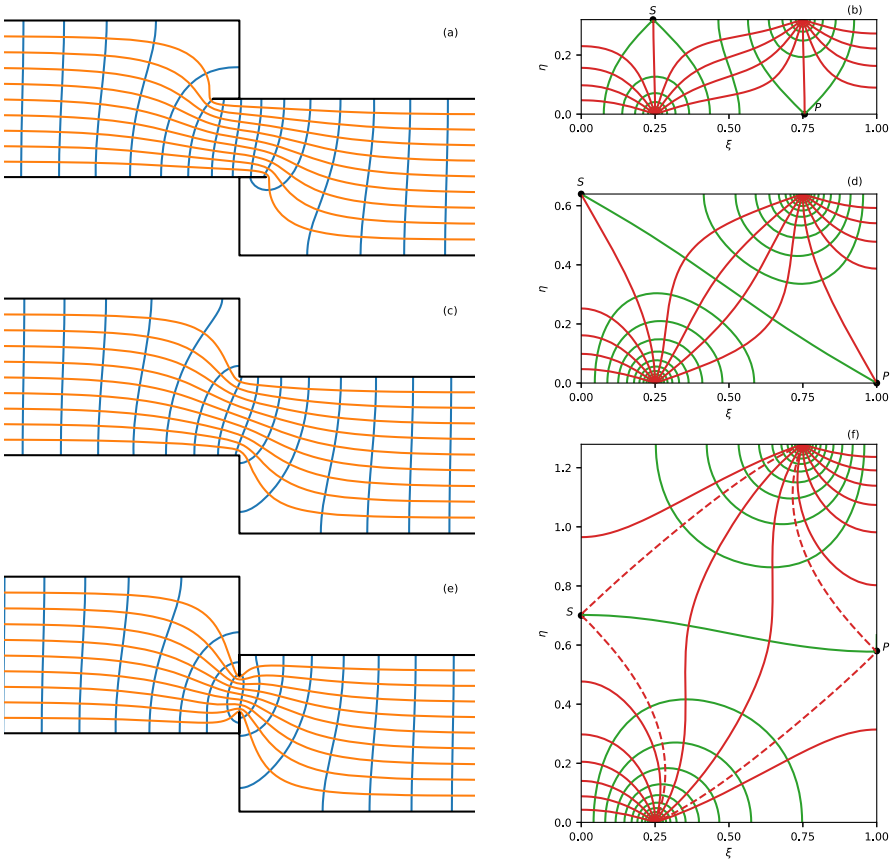

Fig. 7 Flow through a vertical fault. Solutions for different values of B. Flow net (left column) and contour plots of x (green) and y (red) in the reference plane right column. $B/2$, (a) and (b) ; B, (c) and (d); and $2B$, (e) and (f)

resulting flow net are shown as well. The middle row of Fig. 7 is the solution to the stated problem, computed with the value for B such that points 2 and P coincide as well as points 5 and S (Fig. 7c, d). The top row corresponds to the case that the height of the reference plane is $B/2$. Points P and S are visible in the reference plane as stagnation points; point P is located on the bottom boundary of the reference plane between points 1 and 2, and point S is located on the top boundary of the reference plane between points 4 and 5 (Fig. 7b). As a result, sections 1–2 and 4–5 of the boundary of the domain in the physical domain extend horizontally beyond the fault and then loop back over a distance $p = 0.170$ (Fig. 7a). The bottom row corresponds to the case that the height of the reference plane is $2B$ and points P and S are on the right and left boundaries of the reference plane, respectively (Fig. 7f). As a result, sections 2–3 and 5–6 extend vertically into the aquifer in the physical domain over a distance $s = 0.133$ (Fig. 7e).

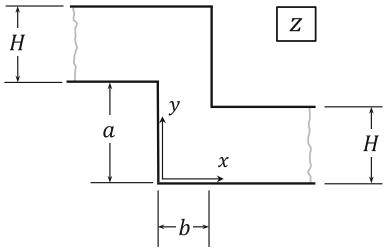

Fig. 8 Definition sketch of an aquifer fold in a vertical plane

4 Example 2: flow through a fold

The solution of Example 1 is modified to simulate flow through a fold, where the top of the aquifer jumps at a different x-location than the bottom of the aquifer (Fig. 8). All parameters are the same as in Example 1, except that the parameter b is chosen non-zero. The conditions for evaluating the mapping parameters are the same as for Example 1, except that (25) becomes

$$z(L) = b + \mathrm{i}H. \tag{28}$$

The value of B is again computed such that $z' = 0$ in point 5. First, consider the case that $\delta = 0.25$ and $b = 0.4$. For this case the top of the aquifer jumps down after the bottom. The shape of the boundary and flow net are shown in Fig. 9a. The resulting value for $B = 1.6838$ and the jump in the base is $a = 1.174$. Second, consider the case that $\delta = 0.15$ and $b = -0.4$. For this case the top of the aquifer jumps down before the bottom of the aquifer. The shape of the boundary and flow net are shown in Fig. 9b. The resulting value for $B = 0.4469$ and the jump in the base is $a = 0.5212$.

5 Example 3: flow through a fault relay ramp

As a final example, consider flow through a fault relay ramp in the horizontal plane (Fig. 10). In the horizontal plane, H represents the width of the aquifer, which is chosen constant ($H_l = H_r = H$). The offset a is more than the width H, and the offset b is positive. The branch points P and S do not coincide with vertices 2 and 5, as they did in the previous two examples. Point 1 is again chosen at $\zeta = \delta$ and point 4 at $\zeta = L - \delta + \mathrm{i}B$, so that the flow field is symmetric. The shape of the fault relay ramp and the flow field are computed for $H = 1$, $b = 2$, $\delta = 0.15$, and $B = 0.6$. The locations of points P and S in the reference plane are obtained from conditions (16) and (17). Point P is located between points 1 and 2 on the bottom of the rectangular reference plane ($\zeta_P = 0.2770$), while point S is located between points 4 and 5 on the top of the reference plane ($\zeta_S = 0.7230 + 0.6\mathrm{i}$). The values of a, p, and s are obtained from Eqs. (18–20), resulting in $a = 1.9$ and $p = s = 1.129$. Finally, the shape of the fault relay ramp and a flow net are shown in Fig. 11.

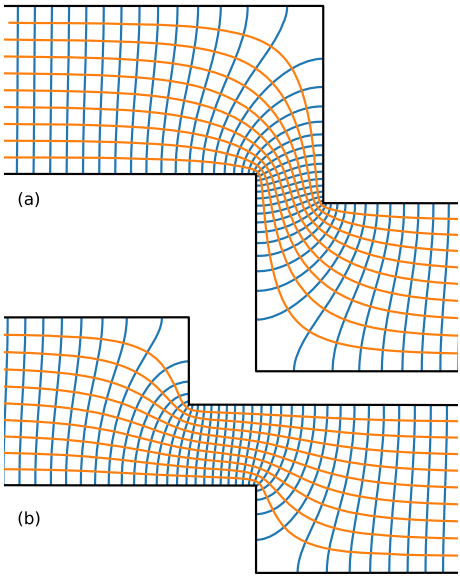

Fig. 9 **a** Flow net for the case that the top of the aquifer jumps down after the bottom ($b = 0.4$ and $\delta = 0.25$) and **b** flow net for the case that the top of the aquifer jumps down before the bottom ($b = -0.4$ and $\delta = 0.15$)

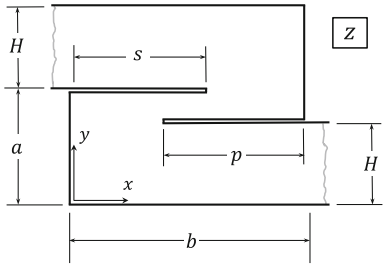

Fig. 10 Definition sketch of a fault relay ramp in a horizontal plane

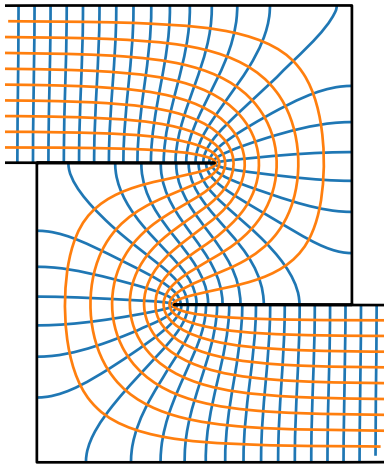

Fig. 11 Flow net for a fault relay ramp in the horizontal plane with $H = 1$, $b = 2$, $\delta = -0.15$, and $B = 0.6$, which gives $a = 1.9$ and $p = s = 1.129$

6 Conclusions

A new potential flow solution was derived for steady groundwater flow through a deformed aquifer. The solution, developed by conformal mapping using the singular point method and a rectangular reference plane, includes several parameters that may be chosen to simulate flow through a variety of deformed aquifer features including faults, folds, and relay ramps. The singular point method allows the development of a very general solution using the basic tools of groundwater mechanics including superposition, the method of images, and stagnation point analysis.

Author contributions Both authors contributed equally to the conceptualization of this paper and wrote the manuscript together. The Python code was written by MB.

Code availability A Jupyter Notebook with Python scripts to reproduce the presented flow nets is available from https://github.com/mbakker7/aquifer_step.

Declarations

Conflict of interest The authors declare no conflict of interest.

References

1. Medici G, Ling F, Shang J (2023) Review of discrete fracture network characterization for geothermal energy extraction. Front Earth Sci 11:1328397
2. Medici G, Smeraglia L, Torabi A, Botter C (2021) Review of modeling approaches to groundwater flow in deformed carbonate aquifers. Groundwater 59(3):334–351
3. Hunt BB, Smith BA, Andrews A, Wierman D, Broun AS, Gary M (2015) Relay ramp structures and their influence on groundwater flow in the Edwards and Trinity aquifers, Hays and Travis counties, Central Texas. In: Proceedings of the 14th conference, Sinklholes and the engineering and environmental impacts of karst
4. Bense V, Gleeson T, Loveless S, Bour O, Scibek J (2013) Fault zone hydrogeology. Earth Sci Rev 127:171–192
5. Goldscheider N (2005) Fold structure and underground drainage pattern in the alpine karst system Hochifen-Gottesacker. Eclogae Geol Helv 98:1–17
6. Caine JS, Evans JP, Forster CB (1996) Fault zone architecture and permeability structure. Geology 24(11):1025–1028
7. Haneberg WC (1995) Steady state groundwater flow across idealized faults. Water Resour Res 31(7):1815–1820
8. Anderson EI (2006) Analytical solutions for flow to a well through a fault. Adv Water Resour 29(12):1790–1803
9. Anderson EI, Bakker M (2008) Groundwater flow through anisotropic fault zones in multiaquifer systems. Water Resour Res 44(11) 1–11

10. Bense VF, Van Balen R (2004) The effect of fault relay and clay smearing on groundwater flow patterns in the Lower Rhine Embayment. Basin Res 16(3):397–411
11. Cornelissen P, Jansen J-D (2023) Steady-state flow through a subsurface reservoir with a displaced fault and its poro-elastic effects on fault stresses. Transp Porous Media 150(3):709–734
12. Gurevich MI (1965) The theory of jets in an ideal fluid. Academic Press, Cambridge
13. Anderson EI (2022) Seepage behind earth retaining structures: the Barros problem revisited. Lobachevskii J Math 43(10):2926–2930
14. Anderson EI (2021) Analytical solutions for confined and unconfined coastal interface flow by the hodograph method. Water Resour Res 57(9):2021–030323
15. Anderson EI (2013) Stable pumping rates for horizontal wells in bank filtration systems. Adv Water Resour 54:57–66
16. Kacimov A (2006) Analytical solution and shape optimization for groundwater flow through a leaky porous trough subjacent to an aquifer. Proc R Soc A Math Phys Eng Sci 462(2069):1409–1423
17. Kacimov A, Obnosov Y (2018) Analytical solution for interface flow to a sink with an upconed saline water lens: Strack's regimes revisited. Water Resour Res 54(1):609–620
18. Muskat M (1946) The flow of homogeneous fluids through porous media, vol 273. JW Edwards Inc., Ann Arbor, MI
19. Bear J (1972) Dynamics of fluids in porous media. Dover, New York
20. Mantoglou A (2003) Pumping management of coastal aquifers using analytical models of saltwater intrusion. Water Resour Res 39(12) 1–7
21. Ding J, Wang S (2018) Analytical solution for 2D inter-well porous flow in a rectangular reservoir. Appl Sci 8(4):586
22. Lu C, Xin P, Li L, Luo J (2015) Steady state analytical solutions for pumping in a fully bounded rectangular aquifer. Water Resour Res 51(10):8294–8302
23. Wang J-Z, Wang X-S, Li Q-B, Wan W-F (2020) Analytical solutions for steady-state multiwell aquifer tests in rectangular aquifers by using double Fourier transform: a case study in the Ordos Plateau, China. Geofluids 2020:1–11
24. Anderson EI (2023) Yield equations for bed-mounted infiltration galleries. J Irrig Drain Eng 149(10):06023003
25. Verruijt A (1970) Theory of groundwater flow. Gordon and Breach, New York, NY
26. Strack ODL (1989) Groundwater mechanics. Prentice Hall, Englewood Cliffs, NJ
27. Bakker M, Post V (2022) Analytical groundwater modeling: theory and applications using Python. CRC Press, New York, NY